SCIENTIFIC REPORTS

OPEN

SUBJECT AREAS:
CANCER
DISEASES

Received
30 April 2014

Accepted
25 June 2014

Published
11 July 2014

Correspondence and requests for materials should be addressed to P.M. (Priyabrata-Mukherjee@OUHSC.edu)

Tuning Pharmacokinetics and Biodistribution of a Targeted Drug Delivery System Through Incorporation of a Passive Targeting Component

Rachel A. Kudgus[1], Chad A. Walden[1], Renee M. McGovern[1], Joel M. Reid[1], J. David Robertson[2] & Priyabrata Mukherjee[3]

[1]Department of Oncology Research, Mayo Clinic, Rochester, Minnesota, United States of America, [2]Department of Chemistry and University of Missouri Research Reactor, University of Missouri, Columbia, Missouri, United States of America, [3]Department of Pathology and Peggy and Charles Stephenson Cancer Center, University of Oklahoma Health Science Center, Oklahoma City, OK, United States of America.

Major challenges in the development of drug delivery systems (DDSs) have been the short half-life, poor bioavailability, insufficient accumulation and penetration of the DDSs into the tumor tissue. Understanding the pharmacokinetic (PK) parameters of the DDS is essential to overcome these challenges. Herein we investigate how surface chemistry affects the PK profile and organ distribution of a gold nanoparticle-based DDS containing both a passive and active targeting moiety via two common routes of administration: intravenous and intraperitoneal injections. Using LC/MS/MS, ELISA and INAA we report the half-life, peak plasma concentrations, area under the curve, ability to cross the peritoneal barrier and biodistribution of the nanoconjugates. The results highlight the design criteria for fine-tuning the PK parameters of a targeted drug delivery system that exploits the benefits of both active and passive targeting.

Nanoparticles have been increasingly explored for various biomedical applications such as detection, diagnosis and therapy[1–5]. Due to its unique ability to bind amine (-NH_2) and thiol (-SH) functionalities, gold nanoparticles (GNPs) provide unique opportunities as a model system to better understand the design criteria for selectively targeting cancer cells *in vitro* and *in vivo*[6]. Gold nanoparticles have been utilized for targeted drug delivery systems (DDS) in an attempt to decrease systemic toxicity, improve efficacy, and alter the bioavailability and clearance of chemotherapeutics. Through proper design and formulation of the chemical and physical properties of the nanoparticle, including surface chemistry and hydrodynamic radius, the pharmacokinetics and biodistribution can be appropriately tailored[7].

Systemic cytotoxicity is a critical limitation of chemotherapeutics. Several approaches have been explored to selectively deliver anti-cancer agents directly to the tumor site. The most widely explored option has been passive targeted drug delivery; utilizing the enhanced permeability and retention (EPR) effect which exploits the leaky tumor vasculature[8]. However, due to the high interstitial fluid pressure, only a fraction of the injected dose (~1%) reaches the tumor site[9]. Vascular normalization therapy using an anti-VEGF antibody has improved the delivery and therapeutic efficacy of anti-cancer agents in a number of cancers[10]. Another approach to selectively deliver chemotherapeutics to the site of the tumor is active targeted drug delivery[11]. In active targeted drug delivery, tumor site-specific delivery of the chemotherapeutics is achieved through incorporation of a ligand or antibody against a surface receptor or antigen usually overexpressed on malignant cells[3,6]. A number of cell surface receptors such as epidermal growth factor receptors (EGFRs), transferrin receptors (TfRs) and folate receptors (FRs) have been explored as targets for tumor specific delivery of chemotherapeutics[3,12,13]. Although a targeted delivery approach significantly improves the site-specific delivery of chemotherapeutics (~10% of the injected dose reaches the tumor site)[14], the study of inhibition of tumor growth and metastasis is not complete.

We hypothesize that incorporation of both an active and passive targeting moiety into a DDS should result in enhanced uptake and therapeutic efficacy by avoiding clearance by the reticuloendothelial systems (RES). Living systems are complex and have both passive and active transport mechanisms[5], which makes it imperative to

investigate both separately and combined. Designing a combination of active and passively targeted DDS will increase circulation time and provide the targeting agent sufficient time to interact with its targets. A detailed investigation of the PK parameters of these delivery systems is essential to understand such processes.

Despite the potential utility for treatment of human disease many nano-based therapies are still in preclinical development[15]. Gold nanoparticles have been utilized for the targeted delivery of several anti-cancer agents including tamoxifen[16], oxaliplatin[17] and gemcitabine[18]. Our lab chose to work with gemcitabine since it is the first line of defense for pancreatic cancer treatment[19]. We developed a designer nanoparticle, ACG44, with the ability to actively target pancreatic cancer cells efficiently and deliver gemcitabine to effectively attenuate tumor proliferation *in vitro* and *in vivo* in an orthotopic model[6,18].

These results motivated us to explore the potential for further improvement of the delivery and efficacy through the investigation of the PK profiles of the particle systems. We sought to overcome some of the barriers observed in nanomedicine, focusing on increasing the bioavailability of the nanoconjugates while examining the influence of size, surface chemistry and mode of administration. We chose to focus on surface modification by adding a small chain length polyethylene glycol (PEG) to investigate the particle transport and potentially reduce the adhesive interactions[18,20]. Intravenous injections need to avoid removal from the circulation by the cells of the reticuloendothelial system (RES), and also need to escape the endothelium in order to enter into the desired target. Intraperitoneal injections are cleared by the lymphatic system or can accumulate in the peritoneum[1]. Herein, we report the nanoparticle formulation, pharmacokinetic analysis, biodistribution and ability to cross the peritoneal barrier of gold nanoparticles formulated with a targeting antibody (cetuximab), gemcitabine and polyethylene glycol (PEG) for a possible improvement in the first line of defense treatment of pancreatic cancer through an active and passive targeting design.

Results

Synthesis and Characterization of ACG44, AIG44 and ACG44p2k nanoconjugates. Physicochemical characterization of ACG44 and AIG44 was previously described[18]. In brief, all nanoconjugates were characterized by UV-visible spectroscopy (UV-vis), transmission electron microscopy (TEM), dynamic light scattering (DLS) and zeta potential (ζ-Potential) measurements.

The UV-vis spectra of unmodified GNPs exhibit a distinctive surface plasmon resonance (SPR) band for ~5 nm spherical gold nanoparticles at a λ_{max} of 512 nm as previously reported[6,18,21]. Adding an antibody to the surface of the GNP increases the absorbance value and exhibits a red shift in the λ_{max}. Specifically, the addition of an anti-EGFR antibody, cetuximab (C225), or its non-targeted counterpart immunoglobulin G (IgG) at a 4 μg/ml concentration to the GNP solution increases the λ_{max} value by increasing the dielectric constant of the solution. The λ_{max} value increases from 512 nm of unmodified GNP to 518 nm for Au-C225 (AC4) and Au-IgG (AI4) conjugates[6,21], respectively. This red shift in the SPR band suggests the binding of the C225 and the IgG to the surface of the GNP as previously reported[6,22]. The optimal concentrations of C225/IgG were 4 μg/ml, these concentrations were selected based on the highest ability to bind to EGFR-overexpressing pancreatic cancer cells both *in vitro* and *in vivo* in an orthotopic pancreatic cancer model as previously described[6]. Based on the targeting efficiency, we designed a targeted drug delivery system. The incorporation of gemcitabine (G) on the AC4 and AI4 nanoconjugates generated ACG44 and AIG44. The optimal concentration of gemcitabine was also 4 μg/ml. The addition of the gemcitabine caused a further red-shift in the λ_{max} from 518 nm to 520 nm for ACG44 and AIG44, suggesting binding of gemcitabine to the available reactive surface on the gold nanoparticle[18].

Both, the *in vitro* and *in vivo* results for the ACG44 nanoconjugates demonstrated significant inhibition of tumor growth in an orthotopic pre-clinical model of pancreatic cancer[18]. To further improve the activity of GNP, we examined the pharmacokinetics of ACG44 and AIG44 and the effect of adding a passive targeting moiety to modulate circulation time. Previous reports indicate that a long plasma half-life can lead to greater target uptake[23], an important goal for any therapeutic, imaging agent or diagnostic material[24]. Passive targeting of nanoparticles exploits this approach based on the enhanced permeability and retention effect[25]. We spectulate that through combining a passive and active targeting system we could eventually design a nanoconjugate with an increased therapeutic effect. To achieve this goal, first, we incorporated a 2 kDa dithiol polyethylene glycol (PEG) to the ACG44 nanoconjugates, producing ACG44p2k. We hypothesized that the addition of the PEG would reduce clearance and maximize the exposure of the nanoconjugate to the target cells. The rationale for adding the 2 kDa PEG in a 5 μg/ml concentration came from previous work in our group[26]. A 5 μg/ml concentration was below 25% of the saturation limit of this PEG on GNPs. The addition of the PEG to the surface of the ACG44 resulted in a blue shift in the SPR band and a λ_{max} value of 514 nm. The stability of ACG44p2k was tested with the addition of NaCl for 15 minutes. It is evident from Figure 1A that although there is a decrease in absorbance of ACG44p2k with the addition of NaCl, there was no broadening of the shape of the curve and there was no shift in the λ_{max} value observed. These results indicate stabilization of the nanoconjugates upon PEG addition. TEM analysis further confirms the absence of aggregation in ACG44, AIG44 and ACG44p2k, as well as the formation of ~5 nm spherical nanoparticles (ACG44p2k is shown in Figure 1B, ACG44 and AIG44 were previously published[18]). Dynamic light scattering (DLS) and zeta potential results were utilized to further characterize the hydrodynamic diameter (HD) and the charge of the particles at each step of conjugation.

A MELVERN Zetasizer Nano ZS instrument was employed for the measurement of both the DLS and ζ-Potentials for all of the nanoconjugates. The average of 5 independent runs is presented in Table 1. As previously reported[18], the HD increases from 5 nm for the unmodified GNP, to approximately 32 nm for ACG44 and 88 nm for AIG44, further demonstrating the binding of C225 and IgG to GNP. The addition of PEG, does not greatly alter the HD of ACG44p2k from ACG44; this observation was expected due to the small relative size of the PEG in comparison to the antibodies; and our previous observations of the HD with the addition of the gemcitabine. The ζ-potential measurements, also previously reported[18], followed a similar trend; the GNP was most negative, with an average of approximately −30 mV. The ζ-Potential starts to become less negative with the addition of C225 and IgG due to the binding and the large size of the antibody. Similarly to the HD, there is only a minor change in ζ-potential with the addition of the PEG.

The ACG44 and AIG44 nanoconjugates were synthesized as previously described[18] and the synthesis of ACG44p2k was simply a further modification to the ACG44 nanoconjugate solution, as described in the materials and methods section. The gold concentrations were consistent across all nanoconjugate injections based on spectrophotometric data. The absorbances obtained at each step of synthesis were confirmed with the known weight of the purchased gold salt. This synthesis was possible due to the spontaneous binding of nearly any amine or thiol-containing molecule exploiting the Au-S/Au-NH_2 bond as previously described[6]. It has been well described in the literature that interactions of proteins, antibodies and small molecules with gold could be due to electrostatics, covalent bonding or hydrophobic interactions[13].

Plasma pharmacokinetics of nanoconjugates affected by particle composition and mode of administration. The blood samples were collected at specific time points, following IP or IV injection, then

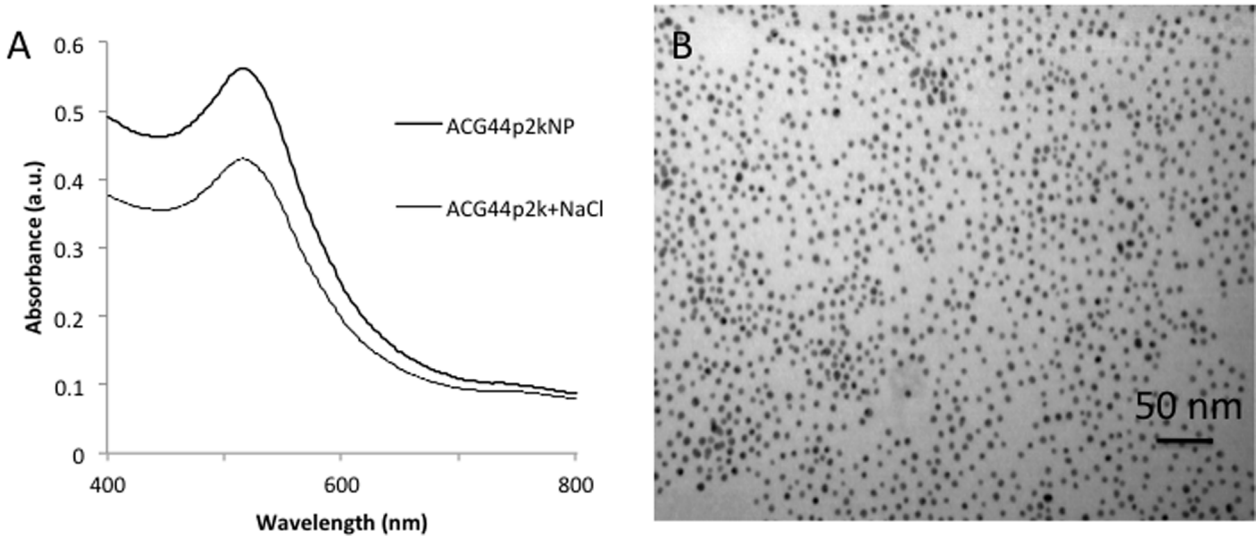

Figure 1 | Physicochemical characterization of gold nanoconjugates. Figure 1A describes the changes in the λ_{max} value of ACG44p2k with/without incubation with NaCl for 15 minutes. Figure 1B exhibits the transmission electron micrographs (TEM) of ACG44p2k nanoconjugates, drop coated after synthesis.

centrifuged to separate the red blood cells from the plasma. The plasma fraction was analyzed for gold, gemcitabine, 2′,2′-difluorodeoxyuridine (dFdU) and when relevant, C225. Plasma concentration-time profiles for each nanoconjugate were analyzed by non-compartmental methods using the program WINNONLIN and are illustrated in Figures 2 and 3, while the pharmacokinetic parameters for gold is summarized in Table 2. Area under the plasma concentration-time curve (AUC) was determined by trapezoidal approximation, using the mean concentration value (n = 3) for each time point. Non-compartmental analysis is typically used as an initial analysis to determine the degree of drug exposure and to compare exposures across different routes of administration[27]. To determine the role of surface chemistry on biological clearance mechanisms, we compared the organ distribution and PK parameters for both IP and IV administered nanoconjugates.

It is evident in Figure 2 that following IP injection the plasma concentrations of free gemcitabine and dFdU are similar for all of the nanoconjugates, regardless of composition. However, the plasma concentrations of non-conjugated gemcitabine are ten-fold higher. This observation implies either a significant stability of the nanoconjugates in mouse plasma releasing only a small amount of gemcitabine or the nanoconjugate cannot freely pass the peritoneal barrier. However, with the incorporation of PEG, the highest peak plasma concentrations (C_{max}) for gold were achieved with ACG44p2k (C_{max} > 80 μg/ml) and the AUC (64560 mg/ml*min). These values were nearly thousand times higher than that of ACG44 and AIG44. These results suggest that the incorporation of PEG to the nanoformulation enhances absorption of the nanoconjugates from the peritoneal cavity to the systemic circulation and increases resident time in the circulation. All analyses are represented up to the detection limit of the HPLC or INAA, respectively.

Table 1 | Dynamic Light Scattering and Zeta Potential Measurements of GNP (the core particle), ACG44, AIG44 and ACG44p2k

Sample	DLS (d.nm)	Zeta Potential (mV)
GNP*	5.3	−29.6
ACG44*	32.09	−20.2
AIG44*	88.95	−20.6
ACG44p2k	36.15	−20.9

Following IV injection, T_{max} (time corresponding to maximum concentration) is achieved for ACG44, AIG44 and ACG442pk within five minutes of the injection, shown in Figure 3. 450 μg of gold was injected for each conjugate at each time point. The C_{max} (maximum concentration) for ACG44 and AIG44 indicates ~5% (20 and 26 μg/ml, respectively) of the injection remains in circulation while nearly 100% (448 μg/ml) remains in circulation for ACG-44p2k. Further corroborating analysis lies in the AUC and CL_p (plasma clearance); the area under the curve and the plasma clearance are substantially different for ACG44p2k. The AUC is 243276 mg/ml*min for ACG44p2k while only ~211 and 293 mg/ml*min for ACG44 and AIG44, indicating longer blood resident time for ACG44p2k. The plasma clearance is ~2 ml/min for ACG44 and AIG44 but 0.00018 ml/min for ACG44p2k, shown in Table 2. Figure 4 shows a representative picture of plasma samples taken from CD1 mice that were injected with ACG44p2k and the corresponding time points. As expected, the addition of the PEG to the nanoconjugates results in dark plasma samples, very similar to the color of the conjugations prior to injection. This observation is consistent with reduced plasma clearance and in turn an increase in the AUC.

Biodistribution of ACG44, AIG44 and ACG44p2k from IP and IV injections. The major RES organs, the liver, spleen and kidneys were excised and analyzed for gold content through INAA. Based on plasma clearance data, two time points, 30 and 240 minutes were examined for gold accumulation from ACG44, AIG44 and ACG-44p2k administered either via IP or IV injections. Figure 5 depicts the percentage of gold retained in these organs for each nanoconjugate and each route of administration. Accumulation in the liver, spleen and kidney varied between IP to IV administration, but was similar for all nanoconjugate types. For IP administration, all organs show a low accumulation of gold after 30 minutes, while there is an expected increase at 240 minutes. It is anticipated that the organ accumulation could be higher for an intravenous injection since the nanoconjugates are injected directly into the blood circulation, as shown in Figure 5. ACG44 and AIG44 appear to have roughly 50% accumulation after 30 minutes and this observation is unchanged at 240 minutes. ACG44p2k shows 25% accumulation after 30 minutes but this nanoconjugate formulation also accumulates to 50% by 240 minutes.

Discussion

Nanotechnology has recently been intensively explored to benefit the medical arena due to the potential to develop new imaging contrast agents, drug delivery systems, and diagnostics[2,3,28]. Decreasing the size of these formulations is exciting and useful for functionality as well as increasing the deliverable payload of a therapy and has been studied with emulsions, liposomes and various metal nanoparticles[2,4]. As described in our recent review, utilizing gold nanoparticles for drug delivery is advantageous based on reproducibility and the flexibility in design[3]. The manipulability of gold nanoparticles could be critical to increasing the efficacy and reducing systemic toxicity of many chemotherapeutics. Previously we demonstrated that a low dose of gemcitabine could be delivered in the form of a gold nanoparticle based targeted drug delivery system to inhibit tumor growth in an orthotopic model of advanced stage pancreatic cancer[18]. Knowing the pharmacokinetics and tissue distribution of nanoparticles conjugates will profoundly dictate the therapeutic effect and toxicity[7,29]. Based on this fact, the purpose of this study was to investigate the pharmacokinetics of this targeted drug delivery system and elucidate the effects of combining active targeting with passive targeting on the pharmacokinetics. To this end, we synthesized and characterized a dual targeting nanoconjugate, ACG44p2k, and explored the pharmacokinetics of differently targeted delivery systems following IV and IP administration. We found that by conjugating gemcitabine to a gold nanoparticle that we could decrease free gemcitabine in circulation and through modifying surface particle chemistry with the addition of PEG we could increase the bioavailability without increasing the accumulation in clearance organs, such as the liver. Enhancing the bioavailability could be beneficial for tumor uptake because it could allow more of the nanoconjugate to be taken up by the targeted cells.

With all nanoconjugates, ACG44, AIG44 and ACG44p2k, thoroughly characterized we were eager to investigate the PK profiles. ACG44 and AIG44 were previously characterized[18]. The red shift we observed with the addition of PEG to the nanoconjugate was consistent with binding and the nanoparticle stability was confirmed through salt testing with physiological salt concentrations, as previously described[18]. Our nanoconjugates are small monodispersed gold nanoparticles with overall charge that is consistent with the range accepted in the literature to have excellent biocompatibility[30]. We found and others have shown that gemcitabine alone is rapidly cleared from plasma[31]. However, by conjugating gemcitabine to the gold nanoconjugate the half-life and clearance are significantly reduced for free circulation gemcitabine. This indicates a low circulating concentration of a cytotoxic chemotherapeutic and could result in lower systemic toxicity; we observed this for all of our nanoconjugate formulations for both IV and IP injections.

Following IP injection, the nanoconjugate must cross the peritoneal barrier that protects the abdominal cavity before entering into the blood stream or accumulating in organs. The peritoneal membrane is a semi-permeable membrane composed of the parietal peritoneum that lines the abdominal wall and the visceral peritoneum that lines the abdominal viscera and internal organs[32]. Both peritoneal membranes are comprised of mucus secreting cells, which we hypothesized is a reason for low bioavailability and nanoconjugate accumulation at these sites following IP administration. Mucus is a complex, viscous biological material that typically serves as a lining, a protective barrier, as well as a lubricant[33]. The Hanes group has utilized low molecular weight polyethylene glycol molecules to penetrate mucus[33].

Polyethylene glycol is a polyether compound and has been shown to mediate particle transport through various biological obstacles such as, adhesive interactions and cytoplasmic hindrances and minimize attractive forces to microtubules, actin filaments and serum albumin[20]. We employed PEG as a passive targeting moiety to reduce the adhesive interactions associated with the mucus in the peritoneum and to facilitate an increased uptake into the blood circulation. PEG has been shown to be safe for use with biological systems[34]; several PEGylated drugs have been approved by the FDA and others

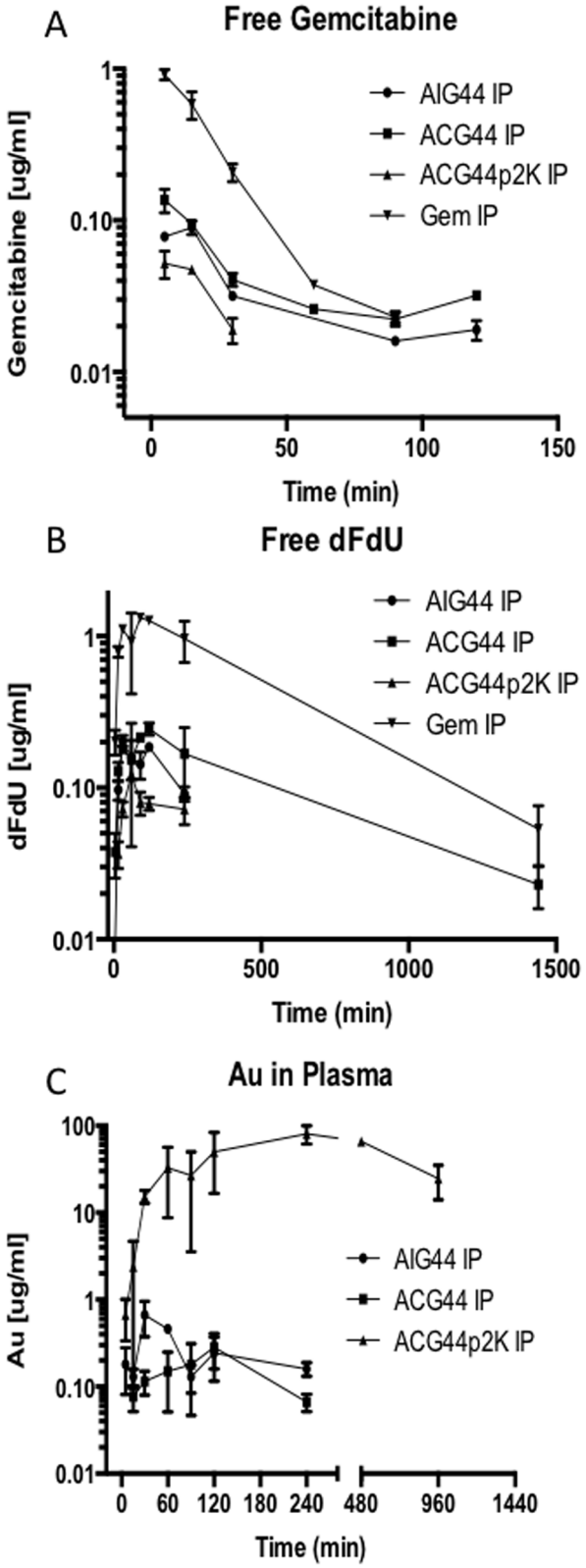

Figure 2 | Concentration/Time Plasma profiles for IP injections. Figure 2A illustrates the free gemcitabine concentration (μg/ml) over time. Figure 2B exhibits the free dFdU concentration (μg/ml) over time. Figure 2C describes gold concentration (μg/ml) over time. Data points are the mean of three animals per time point with standard deviation bars.

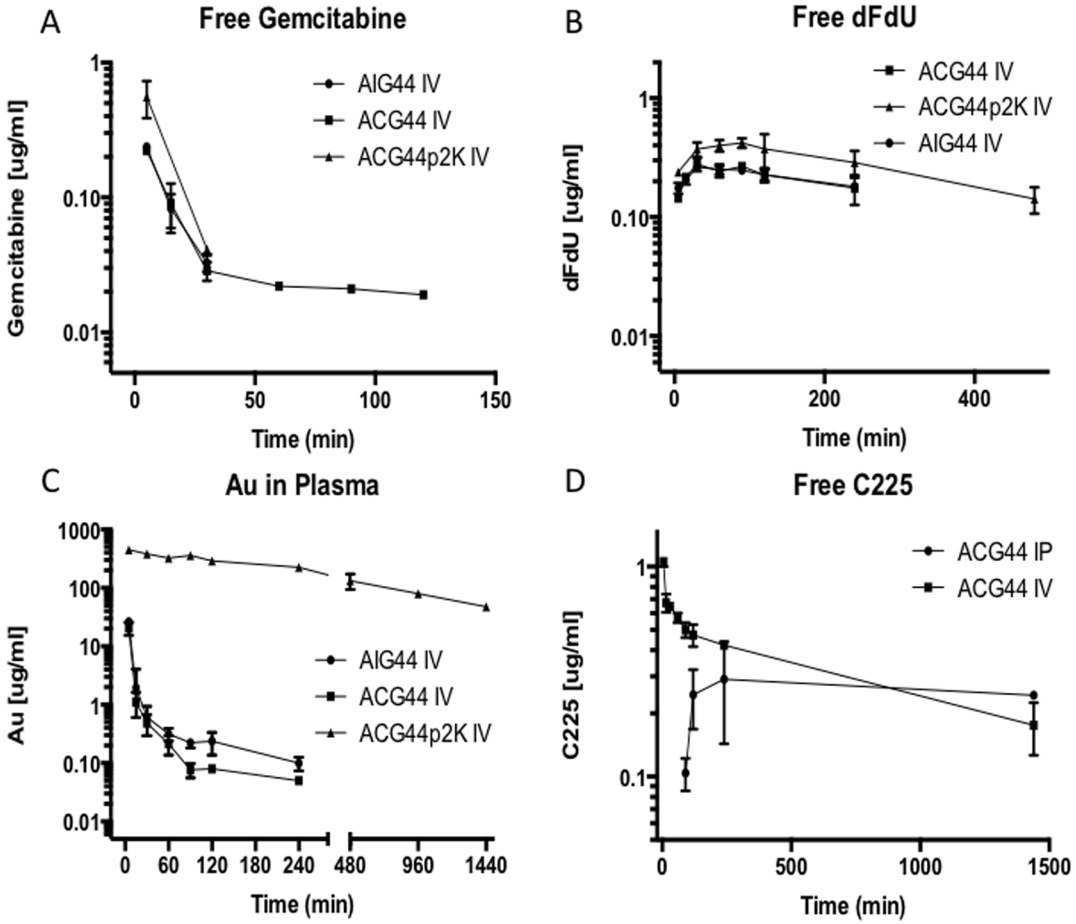

Figure 3 | **Concentration/Time Plasma profiles for IV injections.** Figure 3A illustrates the free gemcitabine concentration (μg/ml) over time. Figure 3B exhibits the free dFdU concentration (μg/ml) over time. Figure 3C describes gold concentration (μg/ml) over time. Figure 3D shows the free C225 concentration (μg/ml) in the plasma after IP and IV injection of ACG44. Data points are the mean of three animals per time point with standard deviation bars.

are being tested in clinical trials[35]. PEGylation presents an important tool for prolonging the blood circulation times[36–39] and by reducing the mononuclear phagocytic system (MPS) or reticuloendothelial system (RES) clearance as a result of minimizing the protein binding to the particle[7,15]. Figure 4 is a digital picture of mouse plasma from mice treated with ACG44p2k IV and the corresponding time point. This image is visual evidence clearly illustrating the retention of the nanoparticle in circulation.

Figure 5 illustrates the organ distribution associated with each nanoconjugate and its respective route of administration. The accumulation seen in the liver could simply be a function of size. Size dependent organ distribution has been investigated and nanoparticles with a hydrodynamic diameter less than 5.5 nm are known to be cleared through the kidneys[40]. Nanoparticles between 50 and 100 nm primarily accumulated in the liver and spleen[41]. However, it has previously been found that gold nanoparticles with long blood circulation times will predominantly collect in the liver[42,43], consistent with our data. Small particles in the range of 30 nm, as ours are, makes them an attractive size because they are small enough to pass through leaky vasculature and demonstrate good blood circulation[15].

In conclusion, we illustrate the differences in pharmacokinetics and organ distribution for three nanoparticle formulations administered both IV and IP. Our data demonstrates that PEG enhances absorption and clearance of the nanoconjugate both through IV and IP administration. Taken together it is evident that incorporation of a PEG-backbone to the DDS enhances absorption into the blood stream from the peritoneal cavity and decreases the plasma clearance, for both IP and IV administration. These findings could be critical to the design and development of a new targeted regime of chemotherapies that enhance the therapeutic efficacy while decreasing the systemic cytotoxicity of the therapy. All in all, pharmacokinetic and biodistribution studies are fundamental aspects for evaluating the safety and suitability of any potential therapeutic. Future work will focus on understanding the targeting and thera-

Table 2 | Pharmacokinetic Parameters based on Gold Analysis

Treatment	C_{max} (ug/ml)	T_{max} (min)	$T_{1/2}$ (min)	$AUC_{0->\infty}$ (mg/ml*min)	CL_p (ml/min)
AIG44 – IP	0.666	30	194.241	107.33	4.19
ACG44 – IP	0.283	120	68.994	48.123	9.35
ACG44p2k – IP	80.513	240	407.683	64560.25	0.00697
AIG44 - IV	26.47	5	113.15	293.04	1.53
ACG44 – IV	20.45	5	219.732	211.808	2.12
ACG44p2k – IV	448.83	5	644.57	243276.58	0.0001849

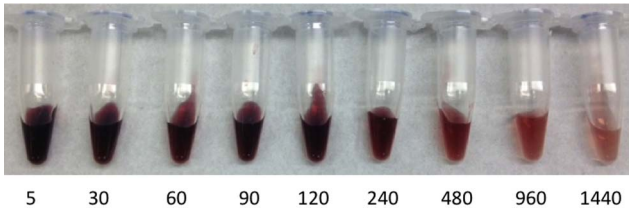

Figure 4 | Digital Image of Mouse Plasma Samples. Representative plasma samples and the corresponding time points from ACG44p2k IV experiment, illustrating prolonged nanoconjugate circulation times with the combination targeting nanoconjugate.

peutic efficacy of these nanoconjugates containing both active and passive targeting moieties to understand the toxicological profiles and their ability to inhibit tumor growth.

Methods

Materials. Tetrachloroauric acid trihydrate, sodium borohydride and poly(ethylene glycol) dithiol were from Sigma-Aldrich, St. Louis, MO. Cetuximab (C225) was purchased in a solution of 2 mg/ml (Erbitux™ Injection, ImClone Inc and Bristol-Myers Squibb Co.) and human IgG was purchased in a solution of 10.0–11.2 mg/ml (Jackson Immuno Research Laboratories, Inc.). Gemcitabine and 2′,2′-difluorodeoxyuridine (dFdU) were purchased in 200 mg vials (Gemzar™, Lilly, Indianapolis, IN). Tetrahydrouridine (THU) 10mg was purchased from Calbiochem (La Jolla, CA). HPLC grade methanol and acetonitrile (EM Science) and monobasic potassium phosphate (Baker-analyzed, J. T. Baker) were used as received. Mouse plasma was purchased from Valley Biomedical (Winchester, VA) and stored frozen at −20°C. Carrier free recombinant human EGFR was purchased from R&D Systems, Inc, (Minneapolis, MN). Nunc Maxisorp 96 well plates, PBS (Phosphate Buffered Saline), TBS (Tris Buffered Saline), Blocker Blotto in TBS, Blocker Casein in TBS, TMB HRP (3,3′,5,5″-tetramethylbenzidine horseradish peroxidase) substrate (BioFX TMBW One Component HRP Substrate) and TMB stop solution (BioFX LSTP 450 nm Stop Solution for TMB) were purchased from Fisher Scientific (Pittsburg, PA). Tween 20 was purchased from Sigma-Aldrich (St Louis, MO). Unconjugated mouse monoclonal antibody to Human IgG1 and peroxidase conjugated mouse monoclonal antibody to Human IgG1 for the ELISA were purchased from Invitrogen Corporation (Camarillo, CA).

Synthesis and characterization of Au-antibody-gemcitabine nanoconjugates and Au-antibody-gemcitabine-PEG nanoconjugates. In brief, as previously described[18] the core gold nanoparticles (GNPs) were synthesized by reduction of a gold salt solution. An aqueous solution of 0.1 mM tetrachloroauric acid trihydrate ($HAuCl_4$) (1200 ml) was reduced with 600 ml of a freshly prepared aqueous solution containing 51.6 mg of sodium borohydride ($NaBH_4$). The solution spun vigorously overnight at room temperature. Upon addition of the sodium borohydride, the pale yellow tetrachloroaurate solution becomes orange and then turns to a wine red color within minutes.

The Au-antibody-gemcitabine nanoconjugates (ACG44 and AIG44) were synthesized as previously described[18], by mixing 4 μg/ml of antibody (C225 or IgG, respectively) with the core GNP solution. After dilution in 1 ml of water each antibody was added dropwise to the GNP solutions. These solutions were stirred vigorously at ambient temperature for 1 hr. After the hour, 4 μg/ml of gemcitabine, also diluted in 1 ml of water was added dropwise and the solutions continued to stir for another hour at ambient temperature.

The Au-antibody-gemcitabine-PEG nanoconjugates (ACG44p2k) were synthesized with one additional step. Poly (ethylene glycol) dithiol (1500 average molecular weight) was added in a 5 μg/ml concentration, also diluted in 1 ml of water and added dropwise to the ACG44 solution and continued to stir vigorously at room temperature for another hour.

All nanoconjugate solutions (ACG44, AIG44 and ACG442pk) were centrifuged at 20,000 rpm in a Beckman Ultracentrifuge in a 50.2 Ti rotor to separate ACG44, AIG44 and ACG44p2k nanoconjugates from unconjugated antibody, gemcitabine and PEG. All conjugates formed a loose pellet at the bottom of the centrifuge tube and were collected after careful aspiration of the supernatant.

The gold concentration of the nanoconjugates was determined from absorbances obtained by UV-visible spectrometry (SpectraMax M5e) at 500 nm (A_{500}) and 800 nm (A_{800}). The absorbances were taken before and after centrifugation and concentrations were determined based on the known weight of the purchased gold and further confirmed by instrumental neutron activation analysis (INAA). The antibody loading was previously determined[6] and the gemcitabine concentration in the nanoconjugates was determined through high-performance liquid chromatography (HPLC) analysis of the supernatant and subtracted from the total μg added to determine the bound concentration as previously reported[18]. All nanoconjugates were characterized by UV-visible spectrometry, scanning from 400–800 nm and transmission electron microscopy (TEM) after drop-coating 10 μl of the sample on a 400 mesh carbon-coated copper grid followed by side blotting. The size and hydrodynamic diameter of the nanoparticle conjugates was determined from analysis of the TEM images and DLS, respectively. Zeta potential measurements were done using a clear zeta disposable capillary (Malvern DTS1061). All characterization was previously published for ACG44 and AIG44[18].

Measurement of gold content by Instrumental Neutron Activation Analysis (INAA). Samples were analyzed by instrumental neutron activation analysis at the University of Missouri Research Reactor Center as previously described[6,44]. Briefly, plasma and tissues were prepared by transferring the samples into high-density polyethylene irradiation vials and lyophilized to a dry weight. All samples were then irradiated for 90 sec in a thermal flux density of approximately 5×10^{13} n cm^{-2} s^{-1}. The samples were then allowed to decay for 24 to 48 hrs and counted on a high-purity germanium detector for 3600 sec at a sample-to-detector distance of approximately 5 cm. The mass of gold in each sample was quantified by measuring 411.8 keV gamma ray from the β^- decay of ^{198}Au ($t_{1/2}$ = 2.7 days). The area of this peak was determined by the Genie ESP spectroscopy package from Canberra and compared to 0.5 μg and 5 μg gold standards irradiated and counted under identical conditions. The gold standards were prepared from certified (High Purity Standards) standard solutions.

Transmission electron microscopy (TEM). TEM samples were generated by drop coating 10 μl of concentrated nanoconjugates, side wicking and rinsing with 10 μl of water. Micrographs were taken on a TECNAI 12 operating at 120 KV[6,18].

Animals. Male CD1 mice (20–25 grams) were purchased from Charles River (Wilmington, MA). All mice were housed and maintained under specific pathogen-free conditions in facilities approved by the American Association for Accreditation of Laboratory Animal Care and in accordance with current regulations and standards of the U.S. Department of Agriculture, U.S. Department of Health and Human Services, and NIH. All studies were approved and supervised by the Mayo Clinic Institutional Animal Care and Use Committee (IACUC Protocol No A10711).

Pharmacokinetics. All nanoconjugates were normalized to a gold concentration of 450 μg/mouse (1.8 mg/kg of gemcitabine) and administered intraperitoneally (IP) in the right side of the abdomen and intravenously (IV) into the lateral tail vein using a 1cc insulin syringe fitted with a $27^5/_8$ gauge needle. The mice were anesthetized under isoflurane vapors at specific time points after injection (5, 15, 30, 60, 90, 120, 240, 480, 960 and 1440 minutes) and sacrificed via cardiac puncture. The anticoagulant solution (approximately 100 μL) consisted of 10% heparin, 1 mg/mL THU in citrate phosphate dextrose. These samples were transferred to microcentrifuge tubes and spun immediately to separate the red blood cells from the plasma (14,000 rpm × 3 min at 4°C). The plasma portion was transferred to fresh microcentrifuge tubes and both the plasma and red blood cells were immediately frozen and stored at −20°C until analysis. Plasma samples were analyzed via INAA for gold content, HPLC for gemcitabine and dFdU concentrations and ELISA for C225 concentrations. All data was analyzed by standard non-compartmental methods using Phoenix WINNONLIN 6.3 (Certara, L.P., St. Louis MO). The apparent terminal elimination rate constants (λz) were determined by linear least-squares regression through the last two plasma-concentration time points for all samples. The apparent elimination half-life ($t_{1/2}$) was calculated as 0.693/λz. Area under the plasma concentration-time curves (AUC_{0-24h}) were determined using the linear trapezoidal rule from time zero to the 24 h sample time. Area under the plasma concentration-time curves through infinite time ($AUC_{0-\infty}$) were calculated by adding CT/λz to AUC_{0-24h}. The CL_p was calculated as dose/($AUC_{0-\infty}$).

HPLC Analysis. Plasma standards were prepared in microcentrifuge tubes by spiking 5 uL of Gemcitabine and dFdU into 190 uL of plasma containing 0.125 mg/mL THU. Floxuridine (10 μL) was added as an internal standard. Gemcitabine and dFdU were isolated by protein precipitation with the addition of 600 μL of acetonitrile. Analyte extraction was carried out via protein precipitation with the addition of 600 uL of acetonitrile. The samples were centrifuged for 5 minutes at 14000 RPM at 25°C. The supernatant was collected, dried under nitrogen, reconstituted with 200 uL of water and vortex mixed. Gemcitabine and dFdU extracted from plasma were quantified by reverse-phase HPLC with UV absorbance detection on a Shimadzu 10 series HPLC system. Separation of gemcitabine, dFdU and the internal standard floxuridine was achieved on an Atlantis T3 C18 column (Waters, 100 mm × 2.1 mm i.d., 5 μm particle diameter) fitted with a Brownlee NewGuard RP-18 pre-column (Chrom Tech, 15 mm × 3.2 mm i.d., 7 μm particle diameter). The mobile phase consisted of 10 mM potassium phosphate, pH 3.0 and methanol. The run was a gradient run starting out with 100% aqueous for 6 minutes, decreasing to 95% aqueous in 7 minutes and holding at 95% aqueous for 4 minutes followed by a high organic wash. The flow rate, the injection volume and detection wavelength were 0.4 ml/min, 20 μL and 272 nm, respectively.

Cetuximab ELISA. Cetuximab was measured using a published ELISA method[45]. Each well of a 96-well plate was coated with 1.65 μg/100 μL of EGFR in PBS. After overnight incubation at 4°C on a rotating platform at 70 RPM the EGFR solution was removed, the wells were washed five times with TBS + 0.05% tween 20 with a 15 second soak between washes on a BioTek ELx50 (BioTek Instruments, Inc, Winooski, VT) plate washer and plates were incubated for 2 hours at room temperature with blocking buffer (300 μL/well; Blocker BLOTTO:Blocker Casein, 20 : 80). After the blocking buffer was removed samples and standards at a 1/100 dilution in blocking

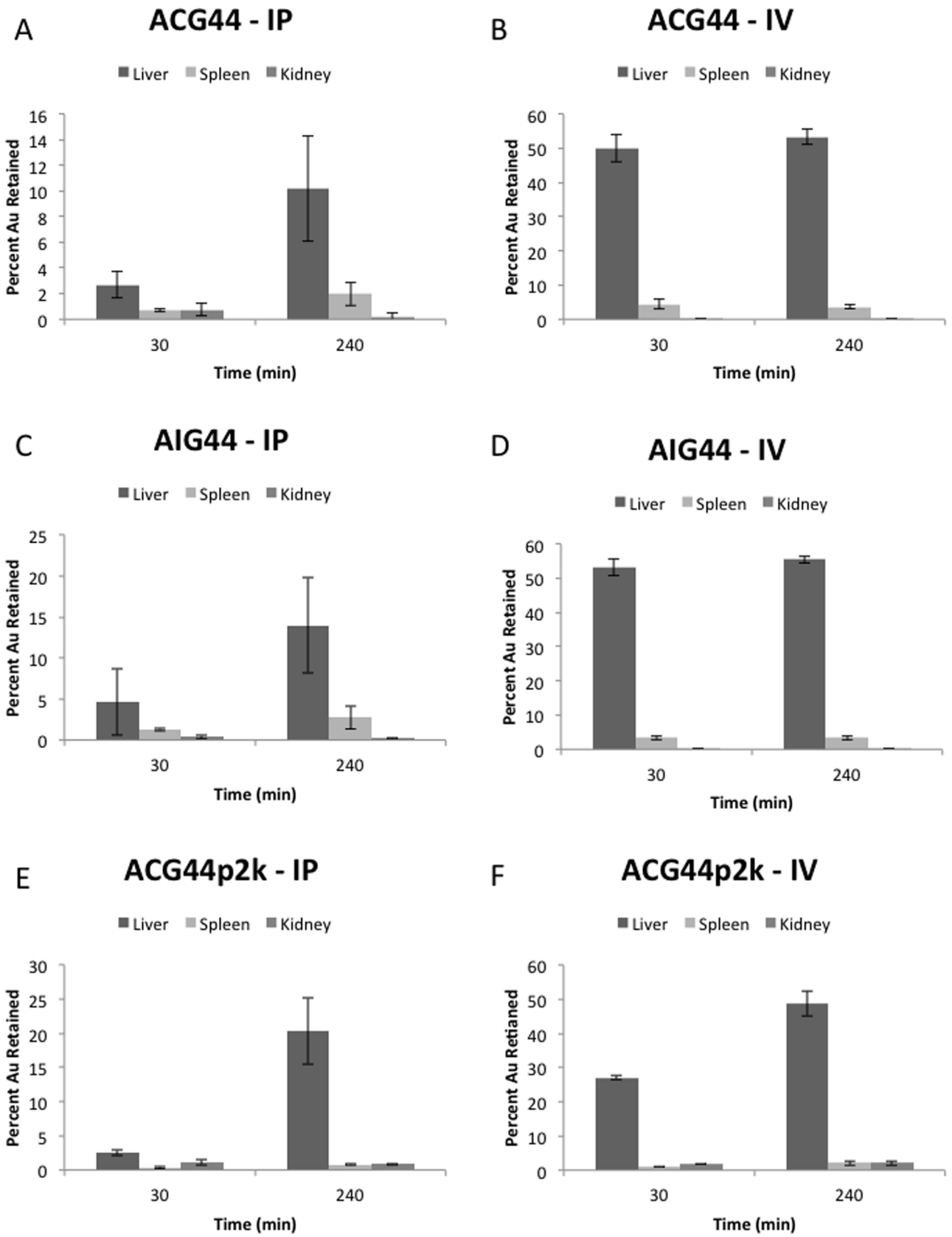

Figure 5 | Bioaccumulation of the nanoconjugates in the liver, spleen and kidneys. Cumulative gold collection concentrations in the liver spleen and kidney. Shown as percent retained from the original injection and measured by INAA. Figure 5A, 5C and 5E all represent IP administration of ACG44 (active targeting nanoconjugate), AIG44 (passive targeting nanoconjugate) and ACG44p2k (combination or active and passive targeting nanoconjugate), respectively. Figure 5B, 5D and 5F all represent IV administration of ACG44 AIG44 and ACG44p2k, respectively.

buffer (100 μL each) were added to the wells. After 1 hour incubation at room temperature, the plate was washed 5 times as described previously and dilute (1/2000 in blocking buffer) secondary antibody at a 1 : 4 mix of conjugated Anti Human IgG1 and unconjugated IgG1 was added to each well and incubated at room temperature for 1 hour. After 5 washes to remove the secondary antibody, plates were incubated at room temperature with cold TMB substrate (100 μL/well) for 20 minutes followed by TMB stop solution (100 μL/well) for 5 minutes. Absorbance was measured on a Molecular Devices Spectro-Max 384 at 450 nm (with 650 nm background subtracted). A 5-parameter logistic fixed weight curve was used for data analysis. The linear range of the standard curve was 0.31 ug/ml to 15 ug/ml.

Biodistribution. After cardiac puncture the liver, spleen and kidneys were collected and immediately frozen on dry ice and stored at −80°C until analyzed for gold uptake through INAA[6,18,44].

Statistical analysis. Statistical analysis was done by a two-tailed student t-test and a value of $P < 0.05$ was considered to be significant.

1. Petros, R. A. & DeSimone, J. M. Strategies in the design of nanoparticles for therapeutic applications. *Nature reviews. Drug discovery* **9**, 615–627, doi:10.1038/nrd2591 (2010).
2. Bhattacharyya, S., Kudgus, R. A., Bhattacharya, R. & Mukherjee, P. Inorganic nanoparticles in cancer therapy. *Pharmaceutical research* **28**, 237–259, doi:10.1007/s11095-010-0318-0 (2011).
3. Kudgus, R. A., Bhattacharya, R. & Mukherjee, P. Cancer nanotechnology: emerging role of gold nanoconjugates. *Anticancer Agents Med Chem* **11**, 965–973 (2011).
4. Arvizo, R. R. *et al.* Intrinsic therapeutic applications of noble metal nanoparticles: past, present and future. *Chemical Society reviews* **41**, 2943–2970, doi:10.1039/c2cs15355f (2012).
5. Doane, T. & Burda, C. Nanoparticle mediated non-covalent drug delivery. *Adv Drug Deliv Rev* **65**, 607–621, doi:10.1016/j.addr.2012.05.012 (2013).
6. Khan, J. A. *et al.* Designing nanoconjugates to effectively target pancreatic cancer cells in vitro and in vivo. *Plos One* **6**, e20347, doi:10.1371/journal.pone.0020347 (2011).
7. Li, S. D. & Huang, L. Pharmacokinetics and biodistribution of nanoparticles. *Molecular pharmaceutics* **5**, 496–504, doi:10.1021/mp800049w (2008).
8. Maeda, H., Nakamura, H. & Fang, J. The EPR effect for macromolecular drug delivery to solid tumors: Improvement of tumor uptake, lowering of systemic toxicity, and distinct tumor imaging in vivo. *Adv Drug Deliv Rev* **65**, 71–79, doi:10.1016/j.addr.2012.10.002 (2013).
9. Lammers, T., Kiessling, F., Hennink, W. E. & Storm, G. Drug targeting to tumors: principles, pitfalls and (pre-) clinical progress. *Journal of controlled release: official journal of the Controlled Release Society* **161**, 175–187, doi:10.1016/j.jconrel.2011.09.063 (2012).
10. Huang, Y., Goel, S., Duda, D. G., Fukumura, D. & Jain, R. K. Vascular normalization as an emerging strategy to enhance cancer immunotherapy. *Cancer Res* **73**, 2943–2948, doi:10.1158/0008-5472.CAN-12-4354 (2013).
11. Fay, F. & Scott, C. J. Antibody-targeted nanoparticles for cancer therapy. *Immunotherapy* **3**, 381–394, doi:10.2217/imt.11.5 (2011).
12. Steichen, S. D. C.-M., Mary; Peppas, Nicholas, A. Vol. 48/3 416–427 (EUROPEAN JOURNAL OF PHARMACEUTICAL SCIENCES, 2013).
13. Mukherjee, P. *et al.* Potential therapeutic application of gold nanoparticles in B-chronic lymphocytic leukemia (BCLL): enhancing apoptosis. *Journal of nanobiotechnology* **5**, 4, doi:10.1186/1477-3155-5-4 (2007).
14. Choi, C. H., Alabi, C. A., Webster, P. & Davis, M. E. Mechanism of active targeting in solid tumors with transferrin-containing gold nanoparticles. *Proc Natl Acad Sci U S A* **107**, 1235–1240, doi:10.1073/pnas.0914140107 (2010).
15. Wang, J., Sui, M. & Fan, W. Nanoparticles for tumor targeted therapies and their pharmacokinetics. *Current drug metabolism* **11**, 129–141 (2010).
16. Dreaden, E. C., Mwakwari, S. C., Sodji, Q. H., Oyelere, A. K. & El-Sayed, M. A. Tamoxifen-poly(ethylene glycol)-thiol gold nanoparticle conjugates: enhanced potency and selective delivery for breast cancer treatment. *Bioconjugate chemistry* **20**, 2247–2253, doi:10.1021/bc9002212 (2009).
17. Brown, S. D. *et al.* Gold nanoparticles for the improved anticancer drug delivery of the active component of oxaliplatin. *Journal of the American Chemical Society* **132**, 4678–4684, doi:10.1021/ja908117a (2010).
18. Kudgus, R. A. *et al.* Inhibiting the growth of pancreatic adenocarcinoma in vitro and in vivo through targeted treatment with designer gold nanotherapeutics. *Plos One* **8**, e57522, doi:10.1371/journal.pone.0057522 (2013).
19. Rathos, M. J., Joshi, K., Khanwalkar, H., Manohar, S. M. & Joshi, K. S. Molecular evidence for increased antitumor activity of gemcitabine in combination with a cyclin-dependent kinase inhibitor, P276-00 in pancreatic cancers. *Journal of translational medicine* **10**, 161, doi:10.1186/1479-5876-10-161 (2012).
20. Suh, J. *et al.* PEGylation of nanoparticles improves their cytoplasmic transport. *International journal of nanomedicine* **2**, 735–741 (2007).
21. Patra, C. R. *et al.* Targeted delivery of gemcitabine to pancreatic adenocarcinoma using cetuximab as a targeting agent. *Cancer Res* **68**, 1970–1978, doi:10.1158/0008-5472.CAN-07-6102 (2008).
22. Mangeney, C. *et al.* Synthesis and properties of water-soluble gold colloids covalently derivatized with neutral polymer monolayers. *J Am Chem Soc* **124**, 5811–5821 (2002).
23. Dobrovolskaia, M. A. & McNeil, S. E. Immunological properties of engineered nanomaterials. *Nature nanotechnology* **2**, 469–478, doi:10.1038/nnano.2007.223 (2007).
24. Medintz, I. L., Uyeda, H. T., Goldman, E. R. & Mattoussi, H. Quantum dot bioconjugates for imaging, labelling and sensing. *Nature materials* **4**, 435–446, doi:10.1038/nmat1390 (2005).
25. Fang, J., Nakamura, H. & Maeda, H. The EPR effect: Unique features of tumor blood vessels for drug delivery, factors involved, and limitations and augmentation of the effect. *Adv Drug Deliv Rev* **63**, 136–151, doi:10.1016/j.addr.2010.04.009 (2011).
26. Bhattacharya, R., Patra, C., Earl, A. & Wang, S. Vol. 3 224–238 (Nanomedicine: Nanotechnology, Biology and Medicine, 2007).
27. Gibaldi, M. & Perrier, D. *Pharmacokinetics, Second Edition (Drugs and the Pharmaceutical Sciences).* 409 (1982).
28. Sardar, R., Funston, A. M., Mulvaney, P. & Murray, R. W. Gold Nanoparticles: Past, Present, and Future. *Langmuir* **25**, 13840–13851 (2009).
29. Simpson, C. A., Huffman, B. J., Gerdon, A. E. & Cliffel, D. E. Unexpected toxicity of monolayer protected gold clusters eliminated by PEG-thiol place exchange reactions. *Chemical research in toxicology* **23**, 1608–1616, doi:10.1021/tx100209t (2010).
30. Zhang, G. *et al.* Influence of anchoring ligands and particle size on the colloidal stability and in vivo biodistribution of polyethylene glycol-coated gold nanoparticles in tumor-xenografted mice. *Biomaterials* **30**, 1928–1936, doi:10.1016/j.biomaterials.2008.12.038 (2009).
31. Masumori, N. *et al.* Measurement of plasma concentration of gemcitabine and its metabolite dFdU in hemodialysis patients with advanced urothelial cancer. *Japanese journal of clinical oncology* **38**, 182–185, doi:10.1093/jjco/hym171 (2008).
32. Goldwyn, R. M. Gray's anatomy. *Plastic and reconstructive surgery* **76**, 147–148 (1985).
33. Lai, S. K., Wang, Y. Y., Wirtz, D. & Hanes, J. Micro- and macrorheology of mucus. *Adv Drug Deliv Rev* **61**, 86–100, doi:10.1016/j.addr.2008.09.012 (2009).
34. Simpson, C. A., Salleng, K. J., Cliffel, D. E. & Feldheim, D. L. In vivo toxicity, biodistribution, and clearance of glutathione-coated gold nanoparticles. *Nanomedicine: nanotechnology, biology, and medicine* **9**, 257–263, doi:10.1016/j.nano.2012.06.002 (2013).
35. Ikeda, Y. & Nagasaki, Y. PEGylation Technology in Nanomedicine. *Adv Polym Sci* **247**, 115–140, doi:Doi 10.1007/12_2011_154 (2012).
36. Lipka, J. *et al.* Biodistribution of PEG-modified gold nanoparticles following intratracheal instillation and intravenous injection. *Biomaterials* **31**, 6574–6581, doi:10.1016/j.biomaterials.2010.05.009 (2010).
37. Woodle, M. C. & Lasic, D. D. Sterically stabilized liposomes. *Biochimica et biophysica acta* **1113**, 171–199 (1992).
38. Owens, D. E., 3rd & Peppas, N. A. Opsonization, biodistribution, and pharmacokinetics of polymeric nanoparticles. *International journal of pharmaceutics* **307**, 93–102, doi:10.1016/j.ijpharm.2005.10.010 (2006).
39. Li, S. D., Chen, Y. C., Hackett, M. J. & Huang, L. Tumor-targeted delivery of siRNA by self-assembled nanoparticles. *Molecular therapy: the journal of the American Society of Gene Therapy* **16**, 163–169, doi:10.1038/sj.mt.6300323 (2008).
40. Choi, H. S. *et al.* Design considerations for tumour-targeted nanoparticles. *Nature nanotechnology* **5**, 42–47, doi:10.1038/nnano.2009.314 (2010).
41. Zhang, X. D. *et al.* Toxicologic effects of gold nanoparticles in vivo by different administration routes. *International journal of nanomedicine* **5**, 771–781, doi:10.2147/IJN.S8428 (2010).
42. Cho, W. S. *et al.* Acute toxicity and pharmacokinetics of 13 nm-sized PEG-coated gold nanoparticles. *Toxicology and applied pharmacology* **236**, 16–24, doi:10.1016/j.taap.2008.12.023 (2009).
43. Balogh, L. *et al.* Significant effect of size on the in vivo biodistribution of gold composite nanodevices in mouse tumor models. *Nanomedicine: nanotechnology, biology, and medicine* **3**, 281–296, doi:10.1016/j.nano.2007.09.001 (2007).
44. Arvizo, R. R. *et al.* Mechanism of anti-angiogenic property of gold nanoparticles: role of nanoparticle size and surface charge. *Nanomedicine: nanotechnology, biology, and medicine* **7**, 580–587, doi:10.1016/j.nano.2011.01.011 (2011).
45. Hantash, J., Smidt, M. & Bowsher, R. R. The development, optimization and validation of an ELISA bioanalytical method for the determination of Cetuximab in human serum. *Anal Methods-Uk* **1**, 144–148, doi:Doi 10.1039/B9ay00027c (2009).

Acknowledgments

The work is supported by NIH grants CA136494 and CA135011 to PM.

Author contributions

R.A.K. performed experiments (nanoparticle synthesis, characterization and animal experiments), analyzed data and wrote the paper; C.A.W. performed animal experiments, H.P.L.C. analysis, analyzed data and wrote the paper; R.M.M. performed ELISA experiments for C225; J.M.R. designed PK experiments, analyzed data and wrote the paper;

J.D.R. analyzed gold content by INAA; P.M. conceived the idea, designed experiments, analyzed data and wrote the paper.

Additional information

Competing financial interests: Authors declare no competing financial conflict of interest. Dr. Mukherjee serves as an academic editor in the journal.

How to cite this article: Kudgus, R.A. *et al*. Tuning Pharmacokinetics and Biodistribution of a Targeted Drug Delivery System Through Incorporation of a Passive Targeting Component. *Sci. Rep.* **4**, 5669; DOI:10.1038/srep05669 (2014).